Available online at www.sciencedirect.com
ScienceDirect
Journal of Molecular Catalysis A: Chemical 275 (2007) 174–182
JOURNAL OF MOLECULAR CATALYSIS A: CHEMICAL
www.elsevier.com/locate/molcata

Physicochemical and catalytic properties of Fe–P ultrafine amorphous catalysts

Baskaran Rajesh, Natarajan Sasirekha, Yu-Wen Chen *

Department of Chemical Engineering, Nanocatalysis Research Center, National Central University, Chung-Li 320, Taiwan, ROC

Received 26 February 2007; received in revised form 16 May 2007; accepted 18 May 2007
Available online 24 May 2007

Abstract

Fe–P ultrafine amorphous alloy particles have been synthesized by chemical reduction of various iron precursors such as $FeCl_2{\cdot}4H_2O$, $FeCl_3{\cdot}6H_2O$, and $Fe(OAc)_2$ under different preparation mediums, viz., H_2O, ethanol/H_2O, and isopropyl alcohol/H_2O. The synthesized materials were characterized by X-ray diffraction, inductively coupled plasma-atomic emission spectroscopy, N_2 sorption, transmission electron microscopy, X-ray photoelectron spectroscopy, and electron diffraction. The results indicated the existence of amorphous nature of Fe–P materials even when the treatment temperature was up to 400 °C. The structure, morphology, and composition of Fe–P nanoalloys have been significantly influenced by the iron precursor and the type of solvent. Dehydrogenation of ethanol has been carried out in order to evaluate the catalytic properties of the Fe–P nanoalloys and related to the surface properties of Fe–P nanoalloys. Sample $Fe_{89.1}P_{10.9}$ prepared with $FeCl_3{\cdot}6H_2O$ in isopropyl alcohol/H_2O solvent showed the highest activity owing to its high surface area and high turnover frequency.

Keywords: Amorphous alloy; Fe–P; Dehydrogenation; Ethanol

1. Introduction

Since the introduction of rapid quenching techniques [1] for producing metal–metalloid amorphous alloys, the metastable materials with short-range ordering structure have attracted a lot of attention due to their superior electronic, magnetic, mechanical, and chemical properties [2,3]. The classical works of Yamashita et al. and Masumoto et al. [4–14] on hydrogenation of carbon monoxide motivated rapid growth in research into amorphous alloy catalysis. Various amorphous alloys have been prepared and employed in catalysis including electrolysis [15,16], hydrogenation [4–9,17–34], hydrogenolysis [8,9], oxidation [35–39], isomerization [28,40], etc. The presence of high concentration of highly coordinatively unsaturated sites on amorphous alloys causes adsorption and surface reactions more easily than on the corresponding crystalline catalysts. In addition, the nonporous nature of these materials effectively eliminates the effects of intraparticle limitations on surface reactions. The amorphous alloys differ from the crystalline alloys bearing similar compositions in their physical, mechanical, and chemical properties. However, one of the significant demerits is the low surface area of amorphous alloys, which limits their use as an industrial catalyst. A number of new methods have been developed to prepare nanosized amorphous alloy catalysts that combine the characteristics of amorphous alloys with a large disorder and nanometer materials with a small size to attain high surface area.

Ultrafine amorphous alloy particles (UAAP) constitute an overlapping area of amorphous alloys [41,3] and nanophase materials [42,43] and hence attracted a great deal of attention due to their interesting intrinsic properties, e.g., short-range order, long-range disorder and high dispersion, as well as their potential applications, e.g., in powder metallurgy, magnetic materials, catalysts and ferrofluids, higher activity, better selectivity and stronger poison resistance in many hydrogenation reactions, particularly [44,45]. UAAP have properties that are of interest in catalysis: (i) the presence of a large number of surface coordinatively unsaturated sites, (ii) the lack of crystal defects, and (iii) the isotropic, single phase nature of the materials. Examples of UAAP include M–B (M = Fe, Co or Ni) [46–53], Ni–P [54–59], Co–P [60], Fe–P–B (M = Cr, Co or Ni) [61,62], Ni–P–B

* Corresponding author. Tel.: +886 3 422751x34203; fax: +886 3 4252296.
E-mail address: ywchen@cc.ncu.edu.tw (Y.-W. Chen).

1381-1169/$ – see front matter © 2007 Elsevier B.V. All rights reserved.
doi:10.1016/j.molcata.2007.05.027

[61,63–65], Fe–Co–B [66], Fe–Ni–B [66,67], Ni–Co–B [68] as well as ultrafine crystalline particles of Co, Co_2B or $Co(BO_2)_2$, and Fe, Fe_2B, Mg, Al, Ni, Pd [69], and Cu.

In general, the most widely used preparation techniques of the amorphous alloy catalysts are the rapid quenching method and chemical reduction method. The latter has its own advantages in the preparation of UAAP over the former; the composition and hence the properties of the catalysts are more adjustable. In particular, the ratio of different elements being not limited to the eutectic composition of the alloy. One of the most prominent methods is to prepare the amorphous alloys by chemical reduction of the metallic ions with hypophosphite ($H_2PO_2^-$) or borohydride (BH_4^-) to form ultrafine metal boride or phosphide amorphous alloy particles, as first reported by van Wonterghem et al. [70] and developed by Linderoth and Mørup et al. [51,52,71]. The powder samples obtained by chemical reduction are highly dispersed to ensure large surface area of the resultant amorphous alloy catalysts, can be compacted in a variety of forms suitable for catalysis and can be used in catalytic test without any pretreatment, which makes them more convenient in catalytic studies.

Fe–P alloys have been electrochemically prepared under relatively simple experimental conditions. The electrochemical deposition of thin films of Fe–P alloys was carried out under various experimental conditions and their composition, structure, and electrochemical properties were investigated and reported [72]. Fdez-Gubieda et al. [73] studied the Fe and P K edges in a series of $Fe_{100-x}P_x$ amorphous alloys and found that changes of short-range order caused by the sample composition were correlated with magnetic properties. Perera et al. [74] synthesized Fe–P nanoparticles from $Fe(acac)_3$ and $P(SiMe_3)_3$ as a pure-phase, discrete particles and reported the effect of the nanosized dimensions on the resultant magnetic properties. A systematic analysis of the effects of B and P concentrations on the pore distribution, coordination number distribution, and the interatomic distance in amorphous Fe–B and Fe–P alloys was investigated by Hoang [75].

The objective of the present study was to achieve an understanding on the effects of preparative methods on the surface properties of Fe–P amorphous alloy catalysts. Dehydrogenation of ethanol was chosen as a test reaction to probe the catalytic behavior. Emphasis was placed on using different iron precursors and solvents which, in combination with characterization techniques, would reveal its influence on the morphology and catalytic activity of Fe–P alloys.

2. Experimental

2.1. Catalyst preparation

A series of Fe–P samples was prepared by a chemical reduction method. Various iron salts such as $FeCl_2{\cdot}4H_2O$, $FeCl_3{\cdot}6H_2O$, and $Fe(OAc)_2$ were used in this study. An iron salt and $NaH_2PO_2{\cdot}H_2O$ were first dissolved in water separately and then mixed at 70 °C under vigorous stirring. The pH of the solution was adjusted to 11 using 50 wt.% aqueous NaOH solution. The aqueous solution of NaH_2PO_2 was slowly added into the aqueous solution of an iron salt at the rate of 10 cm^3/min. The Fe–P brown precipitate was washed with NH_4OH solution followed by deionized water and then with a 95% ethanol solution. The molar ratio of Fe/P in the primary solution was 1:3 for all the samples. In order to study the effect of solvent, water was replaced with 50% ethanol in water and 50% isopropyl alcohol (IPA) in water. Table 1 shows the preparation conditions employed to study the effect of iron precursors and solvents.

2.2. Catalyst characterization

XRD analysis was performed using a Siemens D500 powder diffractometer. The XRD patterns were collected using Cu $K\alpha_1$ radiation (1.5405 Å) at a voltage and current of 40 kV and 30 mA, respectively. The sample was scanned over the range $2\theta = 20–60^\circ$ at a rate of 0.05°/min to identify the amorphous nature. Samples for XRD were prepared as thin layers on a sample holder. Elemental analysis using inductively coupled plasma-atomic emission spectroscopy (ICP-AES) (Jobin-Yvon Company, France, JY-24) was carried out on the Fe–P samples to study the effect of preparation method on the compositions of the samples. In general, the weighed samples were dissolved in nitric acid and diluted with deionized water to concentrations within the calibration range of each element. The standard solutions purchased from Merck were diluted and used to establish the calibration curves. Wavelengths used for elemental analysis were 259.94 and 249.77 nm for Fe and P, respectively. N_2 sorption isotherms were measured at –197 °C using a Micromeritics ASAP 2010 instrument. Prior to the experiments, the samples

Table 1
Composition of Fe–P catalysts under various preparation conditions

Sample notation	Preparation conditions		Bulk composition[a] (atomic ratio)	Fe/P (atomic ratio)	Surface composition[b] (atomic ratio)
	Iron precursor	Solvent			
A	$FeCl_2{\cdot}4H_2O$	H_2O	$Fe_{87.7}P_{12.3}$	7.1	$Fe_{84.5}P_{15.5}$
B	$FeCl_3{\cdot}6H_2O$	H_2O	$Fe_{81.2}P_{18.8}$	4.3	$Fe_{86.3}P_{13.7}$
C	$FeCl_2{\cdot}4H_2O$	EtOH/H_2O (1:1)	$Fe_{71.7}P_{28.3}$	2.5	$Fe_{60.9}P_{39.1}$
D	$Fe(OAc)_2$	EtOH/H_2O (1:1)	$Fe_{82.6}P_{17.4}$	4.7	$Fe_{83.8}P_{16.2}$
E	$Fe(OAc)_2$	IPA/H_2O (1:1)	$Fe_{89.1}P_{10.9}$	8.2	$Fe_{90.1}P_{9.9}$

Fe/P ratio in the starting material = 1:3.
[a] Determined by ICP-AES.
[b] Determined by XPS.

were dehydrated at 100 °C until the vacuum pressure was below 0.1 Pa. The measurement of the surface areas of the samples was achieved by the Brunauerr–Emmett–Teller (BET) method for relative pressures in the range $P/P_0 = 0.05–0.2$. The morphology and particle size of the samples were determined by transmission electron microscopy (TEM) on a JEM-1200 EX II instrument operated at 160 kV. Initially, a small amount of sample was placed into the sample tube filled with a 95% ethanol solution. After agitating under ultrasonic environment for 10 min, one drop of the dispersed slurry was dipped onto a carbon-coated copper mesh (300#) (Ted Pella Inc., California, USA), and dried in an oven at 100 °C for 1 h. XPS spectra were recorded on a Thermo VG Scientific Sigma Probe spectrometer. The XPS patterns were collected using Al Kα radiation at a voltage and current of 20 kV and 30 mA, respectively. The base pressure in the analyzing chamber was maintained in the order of 10^{-9} Torr. The spectrometer was operated at 23.5 eV pass energy. The binding energy of XPS was corrected by contaminant carbon (C 1s = 285.0 eV) in order to facilitate the comparisons of the values among the catalysts and the standard compounds.

2.3. Catalytic activity

The dehydrogenation reaction was carried out in a continuous, U-shaped, quartz microreactor. About 40 mg of fresh catalyst was placed on a layer of quartz wool. The catalyst was first reduced with 5% H_2 in Ar at 250 °C for 30 min. A saturator containing 99.8% ethanol was kept at a constant temperature of 22 °C. Nitrogen was used as a carrier gas at a constant flow rate of 40 ml/min. The experiments were carried out at a constant temperature of 250 °C under atmospheric pressure. To prevent possible condensation of reactant and products, all connection gas lines and valves were analyzed by a China Chromatography 8900F gas chromatograph with a thermal conductivity detector. The column was 5 m long and packed with Hyesep D, which was maintained at 150 °C. Product gas concentrations were determined with a SCSC2.01 integrator by comparing the peak areas with those for a standard mixture.

3. Results and discussion

3.1. Catalysts characterization

The bulk compositions of the as prepared Fe–P nanoalloys prepared using $FeCl_2$ (in H_2O and EtOH/H_2O), $FeCl_3$ (in H_2O), and $Fe(OAc)_2$ (in EtOH/H_2O and IPA/H_2O) were determined by ICP-AES. The outcome of the effect of three protonic solvents and iron precursors on the substitution degree of P for Fe in Fe–P is listed in Table 1. The results show that the preparation methods significantly affected the concentration of phosphorus bonded to the iron metal. Although large amount of phosphate was used, Fe/P ratios in bulk materials were greater than the stoichiometric ratio (Fe_2P or Fe_3P) in most cases. When water was used as a solvent for $FeCl_2$ and $FeCl_3$, the Fe/P atomic ratios were 7.1 and 4.3, respectively. In contrast, in the case of ethanol as a solvent for $FeCl_2$, the Fe/P atomic ratio was 2.5, which proved the influence of solvent on the composition of Fe–P materials. Interatomic distance between Fe–Fe pairs increases with an increase in the P concentration up to 20%. Due to the large size of P atoms, it creates large cavities in Fe–P alloys and tends to disorder the amorphous nature at higher P concentrations, like in Ni–P alloys [75]. The density of Fe–P alloy decreases with an increase in P substitution and the replacement of P atoms reduces the self-diffusion coefficient of Fe atoms. Ethanol in water comparatively increases the concentration of phosphorous in Fe–P than water or IPA/H_2O. It may be due to the different dielectric constant, dissociation constant, viscosity, and thermal conductivity of the solvents [76]. There is no significant trend in the effects of starting materials and solvent used.

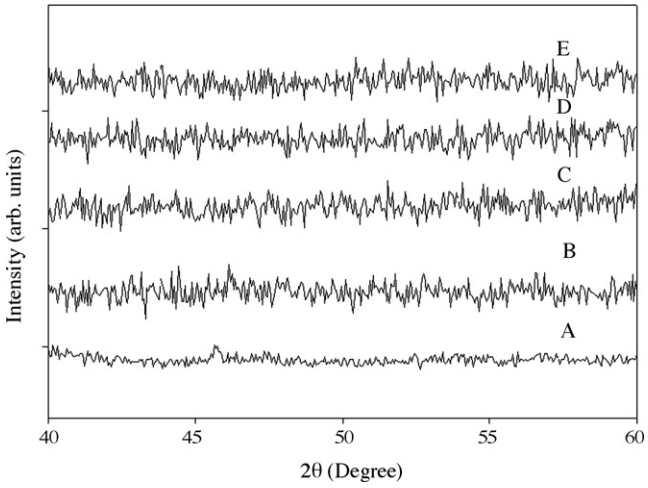

Fig. 1. XRD patterns of Fe–P samples. (A) $Fe_{87.7}P_{12.3}$, (B) $Fe_{81.2}P_{18.8}$, (C) $Fe_{71.7}P_{28.3}$, (D) $Fe_{82.6}P_{17.4}$, and (E) $Fe_{89.1}P_{10.9}$.

Fe–P samples prepared with an Fe/P molar ratio of 1:3 were characterized by XRD to study their crystallinity and phase purity. As shown in Fig. 1, all the Fe–P samples prepared with various Fe precursors and preparation media indicate the amorphous nature of the sample. Thermal treatment of the Fe–P sample was carried out at different temperatures (400 and 500 °C) for 2 h to study the influence of temperature on the structure of Fe–P catalysts. The typical XRD patterns of sample B ($Fe_{81.2}P_{18.8}$) alloys with and without heat treatment are shown in Fig. 2. The as-synthesized sample shows only a broad Fe_α (1 1 0) peak in the XRD pattern, indicating the amorphous nature of the nanoalloy. However, after heat treatment, peaks related to Fe_3P and Fe–P are observed in the XRD patterns along with the Fe_α peak, which indicates the formation of intermetallic phases upon heat treatment. Accordingly, sample B retains its amorphous structure at temperatures below 400 °C and tends to crystallize at 400 °C. From the XRD patterns, it can also be observed that the amorphous Fe–P catalyst gradually separates into two crystalline phases, FeP and Fe_3P. The strength of the diffraction peaks corresponding to Fe_α, FeP, and Fe_3P increased with increase in temperature. During the crystallization process, gathering of small Fe–P particles and rearrangement of the Fe–P particles are expected due to diffusion and migration of the composition elements in Fe–P amorphous alloys. The electron diffraction image (Fig. 3) of sample B further confirms its amorphous nature.

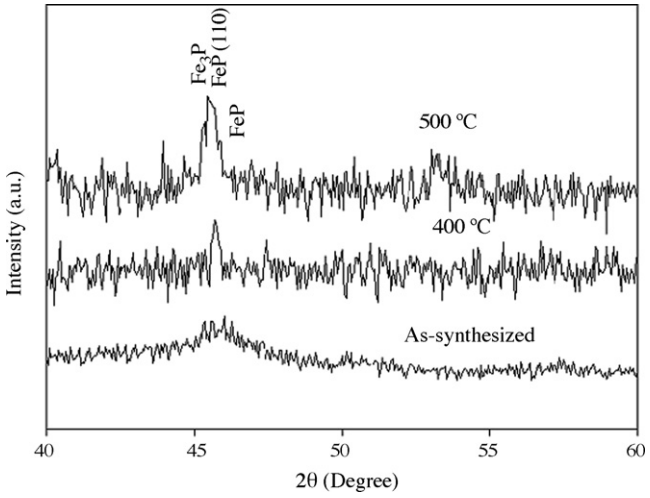

Fig. 2. XRD patterns of sample B upon various treatment temperatures.

The distinct differences in the morphology and particle size of the samples were observed in TEM micrographs. Sample A had a spherical or chain-like morphology with apparent boundary, as shown in Fig. 4. Sample B ($Fe_{81.2}P_{18.3}$) possessed a spherical or needle-like morphology as observed in Fig. 5. A spherical or square morphology was observed for the sample C ($Fe_{71.7}P_{28.3}$) and sample D ($Fe_{82.6}P_{17.4}$) as depicted in Figs. 6 and 7, respectively, while sample E ($Fe_{89.1}P_{10.9}$) had a rectangular morphology (Fig. 8).

Most of the nanoparticles are found to be spherical. Furthermore, by assuming that the Fe–P powder particles are spherical and nonporous, their average sizes can be estimated by the equation: $d\ (\text{nm}) = (6/S_{\text{BET}}\rho) \times 10^3$, where S_{BET} denotes the surface area and ρ represents the density of a particle using the value

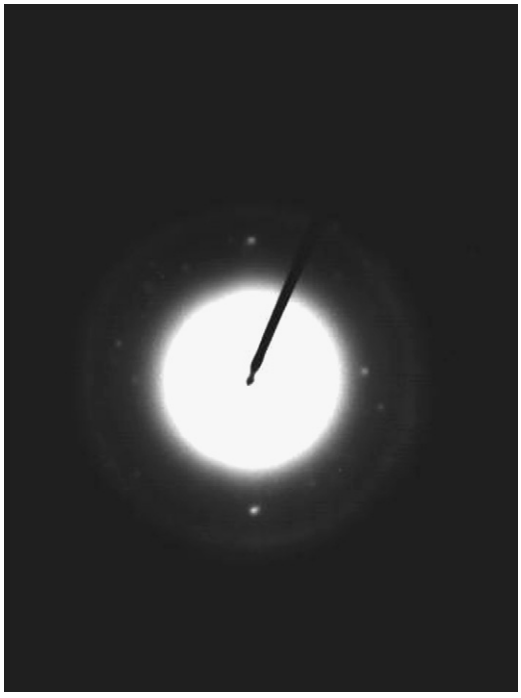

Fig. 3. Electron diffraction image of sample B.

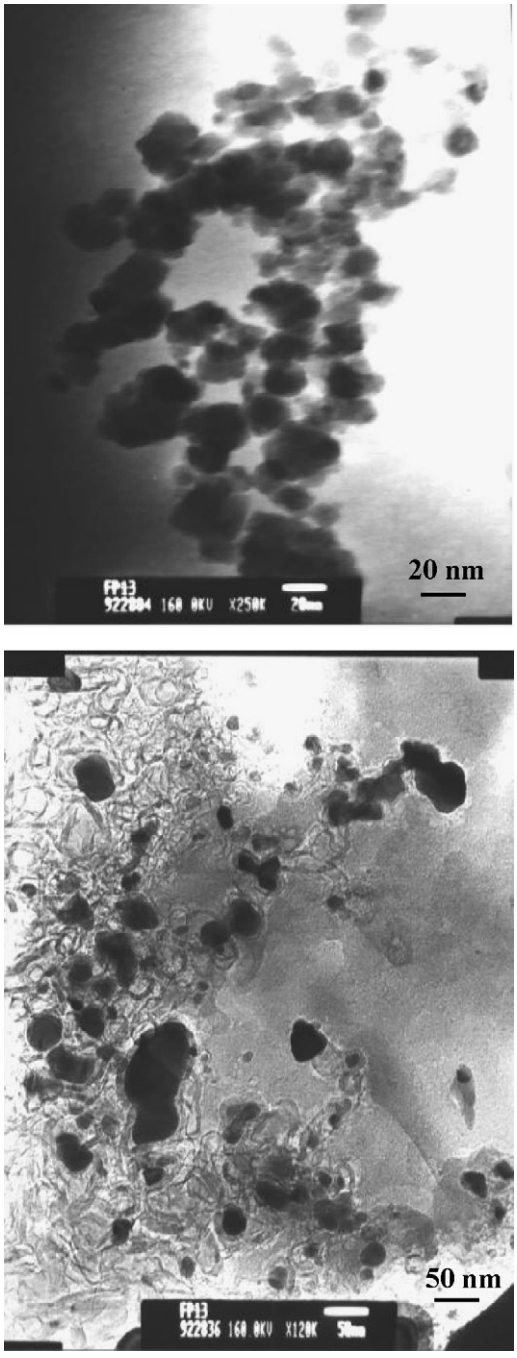

Fig. 4. TEM images of sample A ($FeCl_2$ and H_2O) with spherical or chain-like morphology.

of 7.86 g/cm^3 (the density of iron). The results of particles sizes from TEM micrographs and estimated values from BET surface area resemble each other as tabulated in Table 2. The particle sizes as observed in TEM micrographs are all in nanosize. The particle sizes estimated from BET surface area measurement are in consistency. Sample D prepared with $Fe(OAc)_2$ in $EtOH/H_2O$ solvent demonstrates very high surface area, which has not been reported in literature. In our knowledge, this is the highest surface area of Fe–P prepared by chemical reduction method. The samples were treated at 120 °C before BET surface area measurement. The results of particle size from TEM and those from

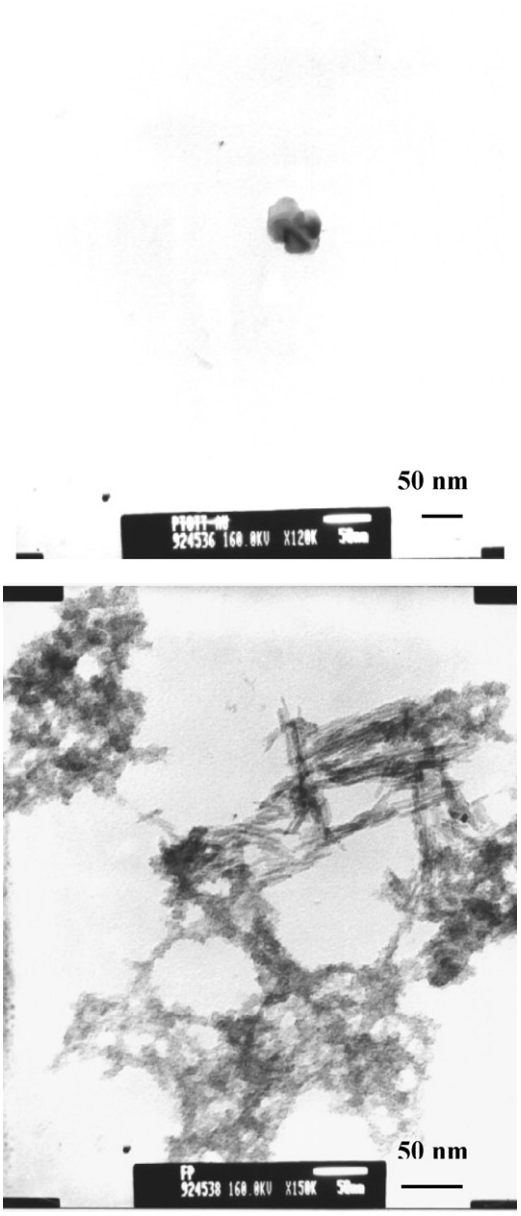

Fig. 5. TEM images of sample B ($FeCl_3$ and H_2O) with spherical or needle morphology.

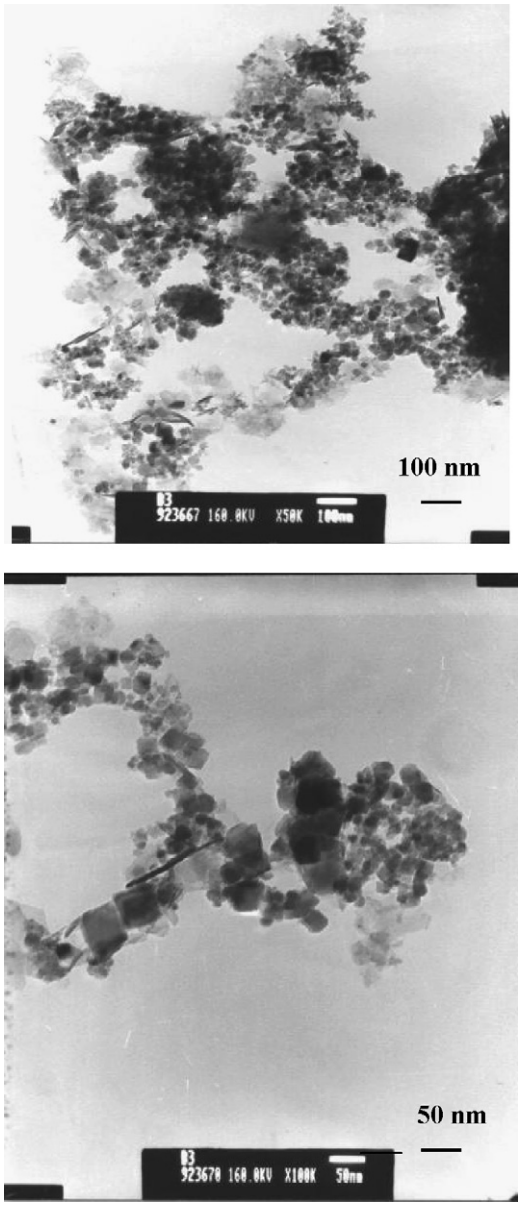

Fig. 6. TEM images of sample C ($FeCl_2$ and $EtOH/H_2O$) with spherical or square morphology.

BET measurement are consistent, which further confirm that the materials did not sinter after treatment at 120 °C. The key point in attaining high surface area of Fe–P is to add the aqueous solution of NaH_2PO_2 very slowly into the aqueous solution of iron salt at the rate of 10 cm^3/min. Most of previous works reported in literature used high feeding rates. The viscosity coefficients of water, ethanol, and IPA are 0.89, 1.08, and 2.00 $\times 10^3$ kg/(m s). The increase in viscosity presumably inhibits the mobility of the reactants thereby giving rise to larger particle size, which is evident from the values presented in Table 2.

Table 2
Surface area and particle size of Fe–P catalysts under various preparation conditions

Catalysts	Surface area (m^2/g)	Particle size (nm)	
		TEM	Estimated average size
A	179	10–20	4.3
B	56	20–30	13.6
C	106	10–20	7.2
D	456	1–10	1.7
E	22	1–50	34.5

The surface compositions of the materials are calculated from XPS spectra by the analysis of relative peak areas. Table 1 reveals that the Fe/P ratios in the starting materials significantly affected the surface compositions of the catalysts. For example, the atomic compositions on the surface and in the bulk were $Fe_{84.5}P_{15.5}$ and $Fe_{87.7}P_{12.3}$, respectively, for sample A. The results concluded that the surface stoichiometry were similar to that of the bulk for Fe–P powder.

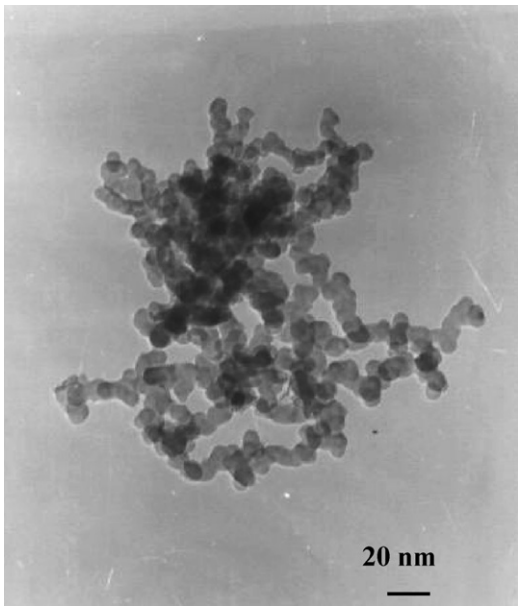

Fig. 7. TEM image of sample D ($Fe(OA_C)_2$ and $EtOH/H_2O$) with spherical or chain-like morphology.

The XPS binding energies of Fe–P catalysts are tabulated in Table 3. Two main peaks of Fe were observed with binding energies of 711.0 and 724.0 eV, attributed to the Fe $2p_{3/2}$ and Fe $2p_{1/2}$ levels, respectively, of Fe 2p core-level due to spin–orbit coupling. The broadening of the Fe $2p_{1/2}$ and Fe $2p_{3/2}$ peaks indicates the existence of Fe^{2+}. The peaks around 711.0 and 724 eV correspond to the Fe 2p components of oxidized iron species such as FeOOH and Fe_2O_3. Similarly, the peaks around 710.0 and 723.1 eV observed after 10 min Ar^+ sputtering could be assigned to Fe_3O_4 and FeOOH species. The XPS spectrum

Fig. 8. TEM image of sample E ($Fe(OA_C)_2$ and IPA/H_2O) with rectangular morphology.

Table 3
XPS binding energy of Fe–P catalysts through different treatments

Fe–P catalysts[a]	Fe (eV)		P (eV)
	$2p_{3/2}$	$2p_{1/2}$	2p
Before Ar^+ sputtering			
A	711.0	724.0	133.1
B	711.0	724.0	133.1
C	711.4	724.3	133.2
D	711.1	724.1	133.1
E	711.0	724.0	133.0
After 10 min Ar^+ sputtering			
A	710.0	723.1	133.0
B	706.4	719.8	129.4
C	710.1	724.1	133.0
D	710.0	724.0	133.0
E[b]	706.8	719.9	129.1

[a] Binding energy was corrected by carbon (C 1s = 285.0 eV).
[b] Sample after 20 min Ar^+ sputtering.

of P 2p core level region shows a peak at 133.1 eV, which can be assigned to the oxidized phosphorus species. From the XPS spectrum recorded after 10 min Ar^+ sputtering, it appears that phosphorus exists in oxidized state in the bulk Fe–P alloy.

Fig. 9 shows the Fe 2p core-level region XPS of sample B and the same after 10 min Ar^+ sputtering. It can be seen that

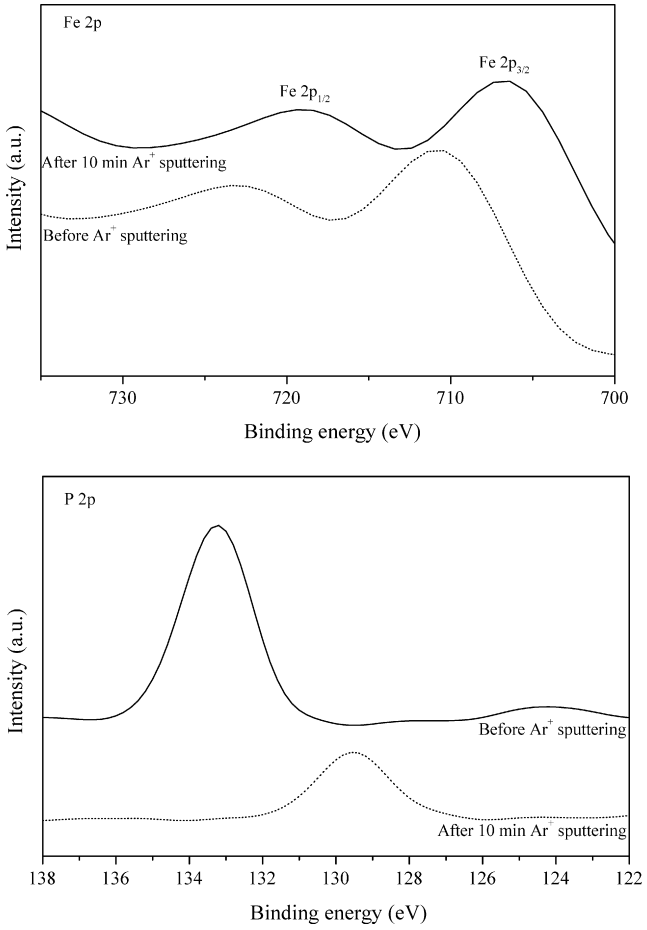

Fig. 9. XPS spectra of sample B.

Fe 2p and P 2p components on the surface of Fe–P catalysts are the same irrespective of the iron precursors and solvents used. Depth profile XPS spectra of the sample showed peaks at 706.4 and 719.8 eV. The binding energy at 706.4 eV is close to that observed for bulk metal iron [77] and the peak at 719.8 eV is characteristic of Fe^{3+}. The binding energy of P 2p is only 129.4 eV, which is close to that of elemental phosphorus (129.1 eV), indicating that metallic iron and phosphorus coexist in the bulk Fe–P alloy. The Fe 2p binding energy of samples C and D corresponds to Fe_3O_4 and FeOOH species, while the peak at 133.1 eV can be assigned to the oxidized phosphorus species. Samples A, C, and D did not show any elemental iron and phosphorus even after sputtering for 10 min.

In sample E, two main peaks of iron observed with binding energies of 706.8 and 719.9 eV are attributed to the Fe $2p_{3/2}$ and Fe $2p_{1/2}$ levels, respectively. The binding energy of 706.4 eV for Fe $2p_{3/2}$ is consistent with that for pure iron metal. The relative areas of the main and shoulder peaks of the Fe $2p_{3/2}$ level suggest that iron is mainly in its metallic state on the bulk of the sample. XPS spectrum of the P 2p level on the bulk of the sample shows a peak with a lower binding energy of 129.1 eV arising from the elemental phosphorus bounded to metallic iron. The binding energy of 129.1 eV for the P 2p level is lower than that of red phosphorus (130.0 eV). The chemical shift of −0.9 eV results from the electron transfer from iron to phosphorus. In conclusion, the starting materials of iron precursor had significant influence on the properties of Fe–P alloys. Metallic iron and phosphorus species are present in the bulk Fe–P alloy prepared using $FeCl_3$ and $Fe(OAc)_2$ in H_2O and IPA/H_2O, respectively, whereas oxidized iron and phosphorus species are present on the surface and bulk Fe–P alloys prepared with $FeCl_2$ (H_2O, EtOH/H_2O) and $Fe(OAc)_2$ (EtOH/H_2O).

3.2. Catalytic activity

Dehydrogenation of ethanol was carried out to compare the catalytic activity of the Fe–P catalysts. The reaction conversions of various preparations of the Fe–P catalysts versus time-on-stream at 250 °C are shown in Fig. 10. The selectivity of acetaldehyde on all the catalysts was nearly 100%. In

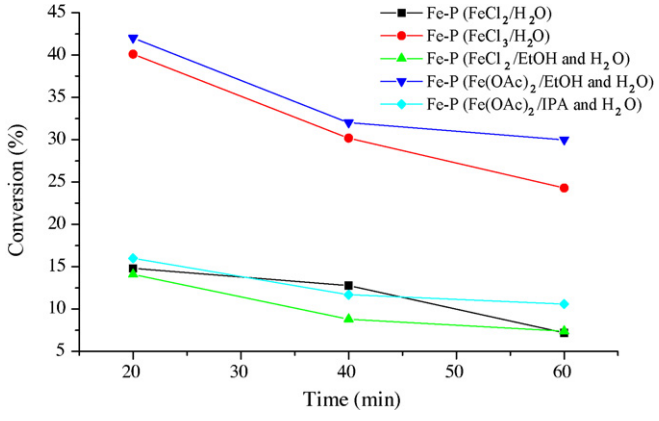

Fig. 10. Reaction conversion on Fe–P catalysts vs. time on stream (reaction condition: 250 °C, F/W = 0.01725 mol ethanol/(g catalyst h)).

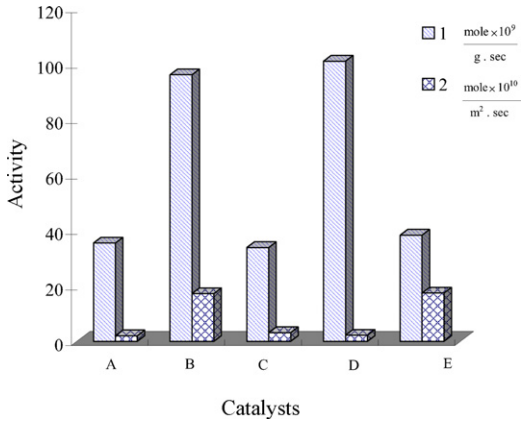

Fig. 11. Dehydrogenation activity of Fe–P catalysts (reaction condition: 250 °C, 1 atm).

this study, the results of all Fe–P catalysts showed deactivation. Sample D gave the highest activity.

The activities of the Fe–P catalysts are exhibited in Fig. 11. For the dehydrogenation of ethanol, the influence of Fe/P mole ratio in the mother solution on the catalytic activity of ultrafine amorphous alloy catalysts can be observed. The catalytic activity per gram of the catalyst was in the following order: D > B > E > A > C. The order of the specific catalytic activity per surface area of the ethanol dehydrogenation (E > B > C > D > A) was manifested. Sample E gave the highest activity among all the catalysts, mainly due to its high surface area. According to our results, the Fe/P molar ratios in the starting materials significantly affect the concentration of phosphorus bonded to the iron metal, subsequently affecting the activity of the catalysts. Experimental results indicated that the different preparation methods significantly affect the surface area and surface composition of the Fe–P catalysts, subsequently affecting the catalytic activity [78]. The specific activity per weight of sample D, prepared with $Fe(OAc)_2$ and EtOH/H_2O showed the highest activity among all the Fe–P catalyst. This catalyst had the highest surface area. In contrast, the specific activity per surface area (named quasi-turnover frequency, QTOF) of sample E, prepared with $Fe(OAc)_2$ and IPA/H_2O showed the highest activity among all the Fe–P catalyst. The high QTOF of this catalyst was possibly due to the high content of metallic iron on the surface; it is known that iron is the active site of the catalyst.

4. Conclusion

Amorphous Fe–P nanoalloy catalysts were prepared by chemical reduction of various iron salts such as $FeCl_2{\cdot}4H_2O$, $FeCl_3{\cdot}6H_2O$, and $Fe(OAc)_2$ under different preparation mediums, viz., H_2O, EtOH/H_2O, and IPA/H_2O. The catalysts were characterized by XRD, TEM, and electron microscopy to confirm the amorphous alloy structure. The results revealed that the use of ethanol led to higher phosphorous concentrations compared with those of the catalysts prepared using water or IPA. The Fe–P samples show the amorphous structure up to 400 °C after which they start to crystallize. The influence of different preparation parameters on the composition and surface morphology

of the alloy particles was investigated in some detail; especially the influence of iron precursor ($FeCl_2$, $FeCl_3$, $Fe(OAc)_2$) and preparation medium (H_2O, EtOH/H_2O, IPA/H_2O) were systematically studied and found to be of vital importance on the physicochemical properties of amorphous Fe–P nanoalloys. XPS results of the catalysts revealed the significant influence of the starting materials of iron salt on the properties of the prepared materials, as evidenced by the metallic iron species obtained when $FeCl_3$ was used, while $FeCl_2$ and $Fe(OAc)_2$ did not result in elemental iron species. Dehydrogenation of ethanol was tested over these catalysts to study their catalytic activity. The selectivity of acetaldehyde on all these catalysts was nearly 100%. Among the catalysts, sample E, prepared using H_2O and IPA, showed the highest activity due to both high surface area and high QTOF. The activity of the catalysts was found to be affected by the different preparation procedures.

Acknowledgments

This research was supported by the Ministry of Economical Affairs, Taiwan, Republic of China, under contract no. 94-EC-17-A09-S1-022.

References

[1] K. Klement Jr., R.H. Willens, P. Duwez, Nature (London) 187 (1960) 869.
[2] M. Shibata, T. Masumoto, Prep. Catal. 4 (1987) 353.
[3] A. Molnar, G.V. Smith, M. Bartok, Adv. Catal. 36 (1989) 329.
[4] S. Yoshida, H. Yamashita, T. Funabiki, T. Yonezawa, J. Chem. Soc., Chem. Commun. (1982) 964.
[5] S. Yoshida, H. Yamashita, T. Funabiki, T. Yonezawa, J. Chem. Soc., Faraday Trans. I 80 (1984) 1435.
[6] H. Yamashita, M. Yoshikawa, T. Funabiki, S. Yoshida, J. Chem. Soc., Faraday Trans. I 81 (1981) 2485.
[7] H. Yamashita, T. Faminade, T. Funabiki, S. Yoshida, J. Mater. Sci. Lett. 4 (1985) 1241.
[8] H. Yamashita, M. Yoshikawa, T. Funabiki, S. Yoshida, J. Chem. Soc., Faraday Trans. I 82 (1986) 1771.
[9] H. Yamashita, T. Funabiki, S. Yoshida, J. Chem. Soc., Chem. Commun. (1984) 868.
[10] S. Yoshida, H. Yamashita, T. Funabiki, Hyomen 24 (1986) 349.
[11] H. Yamashita, M. Yoshikawa, T. Funabiki, S. Yoshida, J. Catal. 99 (1986) 375.
[12] M. Shibata, Y. Ohbayashi, N. Kawata, T. Masumoto, K. Aoki, J. Catal. 96 (1985) 296.
[13] A. Yokoyama, H. Komiyama, H. Inoue, T. Masumoto, H.M. Kimura, J. Catal. 68 (1981) 355.
[14] A. Yokoyama, H. Komiyama, H. Inoue, T. Masumoto, H.M. Kimura, J. Chem. Soc. Jpn. 2 (1982) 199.
[15] M.M. Jaksic, Electrochim. Acta 29 (1984) 1539.
[16] M.M. Jaksic, J. Mol. Catal. 38 (1986) 161.
[17] J.F. Deng, H.Y. Chen, X.H. Bao, M. Muhler, Appl. Surf. Sci. 81 (1994) 341.
[18] J.F. Deng, H.Y. Chen, J. Mater. Sci. Lett. 12 (1993) 1508.
[19] J. Chen, G. Lu, L. Ma, Fudan Univ. Acta 28 (1989) 78.
[20] H.M. Wang, Z.B. Yu, H.Y. Chen, J. Yang, J.F. Deng, Appl. Catal. A 129 (1995) L143.
[21] Z.B. Yu, M.H. Qiao, H.X. Li, J.F. Deng, Appl. Catal. A 163 (1997) 1.
[22] J. Yang, Ph.D. Dissertation, Fudan Univ., 1993.
[23] H.Y. Chen, Ph.D. Dissertation, Fudan Univ., 1994.
[24] J.F. Deng, J. Yang, S. Sheng, J. Catal. 150 (1994) 434.
[25] Z. Hu, J. Shen, Y. Chen, M. Lu, Y.F. Hsia, J. Non-Cryst. Solids 159 (1993) 88.
[26] G. Carturan, G. Cocco, E. Baratter, G. Navazio, C. Antonione, J. Catal. 90 (1984) 178.
[27] A. Baiker, H. Baeis, H.J. Guntherodt, Appl. Catal. 22 (1986) 389.
[28] W.E. Beower, M.S. Matyjaszczyk, T.L. Pettit, G.V. Smith, Nature (London) 301 (1983) 497.
[29] A. Molnar, G.V. Smith, M. Bartok, J. Catal. 101 (1986) 540.
[30] A. Molnar, G.V. Smith, M. Bartok, J. Catal. 101 (1986) 67.
[31] R. Haurert, P. Oelhafen, R. Schlogl, H.-J. Guntherodt, Solid State Commun. 55 (1985) 583.
[32] M. Funakoshi, H. Komiyama, H. Inoue, Chem. Lett. (1985) 245.
[33] A. Baiker, H. Baeis, H.J. Guntherodt, Chem. Commun. (1986) 930.
[34] C.S. Brooks, F.D. Lemkey, G.S. Golden, Mater. Res. Soc. Symp. Proc. 8 (1982) 397.
[35] K. Machida, M. Enyo, Chem. Lett. (1985) 75.
[36] K. Machida, M. Enyo, Bull. Chem. Soc. Jpn. 58 (1985) 2043.
[37] K. Machida, K. Yoshida, M. Enyo, Y. Toda, T. Masumoto, J. Less-Commun. Met. 119 (1986) 143.
[38] K. Machida, M. Enyo, K. Kai, K. Suzuki, J. Less-Commun. Met. 100 (1984) 377.
[39] K. Machida, M. Enyo, I. Toyoshima, Y. Toda, T. Masumoto, Surf. Coat. Technol. 27 (1986) 359.
[40] G.V. Smith, W.E. Beower, O. Zahraa, A. Molnar, M.M. Khan, B. Rihter, J. Catal. 83 (1983) 238.
[41] W.L. Johnson, Progr. Mater. Sci. 30 (1986) 81.
[42] G.C. Hadjipanayis, R.W. Siegel (Eds.), Nanophase Materials, Synthesis–Properties–Applications, NATO ASI Series, Kluwer Academic Publishers, Dordrecht, 1996.
[43] D.L. Bourell (Ed.), Synthesis and Processing of Nanocrystalline Powder, The Minerals, Metal, Materials Society, 1994.
[44] J.F. Deng, H. Li, W. Wang, Catal. Today 51 (1999) 113.
[45] Z. Liu, W.-L. Dai, B. Liu, J.-F. Deng, J. Catal. 187 (1999) 253.
[46] H. Li, Q. Zhao, Y. Wan, W. Dai, M. Qiao, J. Catal. 244 (2006) 251.
[47] Z. Jiang, H.W. Yang, Z. Wei, Z. Xie, W.J. Zhong, S.Q. Wei, Appl. Catal. A 279 (2005) 165.
[48] B.J. Liaw, S.J. Chiang, C.H. Tsai, Y.Z. Chen, Appl. Catal. A 284 (2005) 239.
[49] H.X. Li, Y.D. Wu, J. Zhang, W.L. Dai, M.H. Qiao, Appl. Catal. A 275 (2004) 199.
[50] L.J. Wang, W. Li, M.H. Zhang, K.Y. Tao, Appl. Catal. A 259 (2004) 185.
[51] J. Fang, X.Y. Chen, B. Liu, S.R. Yan, M.H. Qiao, H.X. Li, H.Y. He, K.N. Fan, J. Catal. 229 (2005) 97.
[52] S. Linderoth, S. Mørup, J. Appl. Phys. 67 (9) (1990) 4472.
[53] S. Linderoth, S. Mørup, J. Appl. Phys. 69 (8) (1991) 5256.
[54] J. Saida, A. Inoue, T. Masumoto, Metall. Trans. A22 (1991) 2125.
[55] J.Y. Shen, Z.Y. Li, Q.J. Yan, Y. Chen, J. Phys. Chem. 97 (1993) 8564.
[56] J. Shen, Q. Zhang, Z. Li, Y. Chen, J. Mater. Sci. Lett. 15 (1996) 715.
[57] J. Deng, X. Zhang, Appl. Catal. 37 (1988) 339.
[58] Z. Hu, J.Y. Shen, Y. Chen, M. Lu, Y.F. Hsia, J. Noncryst. Solids 159 (1993) 88.
[59] X. Yan, J. Sun, Y. Wang, J. Yang, J. Mol. Catal. A 252 (2006) 17.
[60] J. Deng, X. Zhang, Solid State Ionics 32 (1989) 1006.
[61] J. Shen, Z. Hu, Y. Hsia, Y. Chen, J. Phys.: Condens. Matter 4 (1992) 6381.
[62] Z. Hu, Y. Fan, Y. Wu, Q. Yan, Y. Chen, J. Magn. Magn. Mater. 140-144 (1995) 413.
[63] S.P. Lee, Y.-W. Chen, Ind. Eng. Chem. Res. 35 (1999) 2548.
[64] S.P. Lee, Y.-W. Chen, J. Chem. Technol. Biotechnol. 75 (2000) 1073.
[65] S. Wells, S.W. Charles, S. Mørup, S. Linderoth, J. Phys.: Condens. Matter 1 (1989) 8199.
[66] H. Li, H. Li, W. Dai, M. Qiao, Appl. Catal. A 238 (2003) 119.
[67] S. Mørup, S.A. Sethi, S. Linderoth, C. Bender Koch, M.D. Bentzon, J. Mater. Sci. 27 (1992) 3010.
[68] H. Wang, Z. Yu, H. Chen, J. Yang, J. Deng, Appl. Catal. A 129 (1995) L143.
[69] Z. Xiong, Z. Mi, X. Zhang, Catal. Commun. 8 (2007) 571.
[70] J. van Wonterghem, S. Mørup, C.J.W. Koch, S.W. Charles, S. Wells, Nature 322 (1986) 622.

[71] S. Linderoth, S. Mørup, A. Meagher, J. Larsen, M.D. Bentzon, B.S. Clausen, C.J.W. Koch, S. Wells, S.W. Charles, J. Magn. Magn. Mater. 81 (1989) 138.
[72] S.K. Zećević, J.B. Zotović, S.Lj. Gojković, V. Radmilović, J. Electroanal. Chem. 448 (1998) 245.
[73] M.L. Fdez-Gubieda, A. García-Arribas, J.M. Barandiarán, J. Herreros, Physica B 208–209 (1995) 363.
[74] S.C. Perera, P.S. Fodor, G.M. Tsoi, L.E. Wenger, S.L. Brock, Chem. Mater. 15 (2003) 4034.
[75] V.V. Hoang, Physica B 348 (2004) 347.
[76] D.R. Lide, Handbook of Chemistry and Physics, CRC Press, Boston, MA, 1990.
[77] A.M. Visco, F. Neri, G. Neri, A. Donato, C. Milone, S. Galvagno, Phys. Chem. Chem. Phys. 1 (1999) 2869.
[78] B.S. Liu, P.Y. Lian, X.H. Zhao, Sep. Purif. Technol. 32 (2003) 281.